

Characterization of finite-time Lyapunov exponents and vectors in two-dimensional turbulence

Guillaume Lapeyre^{a)}

Program in Atmospheric and Oceanic Sciences, G.F.D.L., Princeton University, Forrestal Campus,
P.O. Box 308, Princeton, New Jersey 08542

(Received 7 February 2002; accepted 19 June 2002; published 21 August 2002)

This paper discusses the application of Lyapunov theory in chaotic systems to the dynamics of tracer gradients in two-dimensional flows. The Lyapunov theory indicates that more attention should be given to the Lyapunov vector orientation. Moreover, the properties of Lyapunov vectors and exponents are explained in light of recent results on tracer gradients dynamics. Differences between the different Lyapunov vectors can be interpreted in terms of competition between the effects of effective rotation and strain. Also, the differences between backward and forward vectors give information on the local reversibility of the tracer gradient dynamics. A numerical simulation of two-dimensional turbulence serves to highlight these points and the spatial distribution of finite time Lyapunov exponents is also discussed in relation to stirring properties. © 2002 American Institute of Physics. [DOI: 10.1063/1.1499395]

The mixing properties of passive scalars in time-dependent flows depend very strongly on the chaotic nature of Lagrangian particle trajectories. The more rapidly particles separate from each other, the more efficient mixing can be since a patch of tracer will be stretched into filaments of small width that will spread and mix through the entire fluid. The stretching process of a patch of tracer is equivalent to the growth of the tracer gradient and ideas of dynamical systems can be applied. Here we follow this approach and compare results from Lyapunov theory to results concerning the tracer gradient dynamics in a two-dimensional turbulent flow. Lyapunov exponents were extensively used for this kind of problem but we stress here the importance of Lyapunov vectors. These vectors give information on the different properties of stirring for finite times, such as local reversibility (or “chaoticity”) of the tracer gradient dynamics.

I. INTRODUCTION

An important property of two-dimensional time-dependent flows is that Lagrangian particles can display chaotic trajectories, even in the case of simple Eulerian velocity fields. Close particles separate very quickly from each other and tracer patches spread rapidly to fill the entire chaotic region.^{1–5} This phenomenon is referred to as “chaotic advection.”^{6,7} The strong dispersion of particles results in a nonlocal mixing as opposed to local diffusive mixing. A natural way to quantify this chaotic nondiffusive mixing is to compute the exponential rate of particle separation. The exponent is called Lyapunov exponent by analogy with Lyapunov theory in dynamical systems. This theory states that in the asymptotic limit in time, fluid particles separate with the same exponential growth rate (except maybe for a

region of zero measure) which depends only on the global dynamical properties of the flow. However the mixing properties (for instance, transport barriers, hyperbolic points) depend on the local properties of the flow, i.e., on finite time integration of the Lagrangian trajectories. The extension of Lyapunov theory to finite times is nontrivial, but some progress has been made to introduce finite time Lyapunov exponents^{8,9} (FTLEs). In contrast to the asymptotic exponents, the finite time exponents depend on the initial positions of the trajectories as well as the time of integration of these trajectories. In that sense, they are able to measure the stretching induced by the flow topology and they bear the fingerprints and the persistence in time of the structures that control the stirring processes. Another approach to chaotic mixing is related to the theory of invariant manifolds and was initially developed for time periodic flows.^{10,11} These manifolds are special trajectories that serve as templates for the geometry of mixing. Different attempts have been made to extend this theory to aperiodic flows^{12,13} and some *ad hoc* procedures have been proposed to compute finite time manifolds.^{14,15} A last approach consists in studying the dynamics of the tracer gradient vector.^{16,17} Actually, the orientation of the tracer gradient can be estimated from the flow topology, i.e., through the velocity and acceleration gradient tensors. These different approaches seem to be unrelated at first sight but are actually closely linked together. An example of this relation is that, for periodic flows, the convergence of the orientation of tracer gradient on the Poincaré map allows the determination of the invariant manifolds.¹⁸ Another example is the theorem by Haller¹⁹ that gives a rigorous proof of the criterion proposed by Lapeyre *et al.*¹⁵ to diagnose invariant manifolds based on the dynamics of the tracer gradient orientation. However a general approach involving all of these concepts is still needed to understand finite time properties of chaotic mixing in aperiodic flows.

In this paper, our motivation is to tighten the link between alignment properties of tracer gradients in two-

^{a)}Electronic mail: gnl@gfdl.noaa.gov

dimensional aperiodic flows and Lyapunov theory. Since, in our view, two-dimensional turbulence represents the most challenging test case for mixing and stirring ideas, we will use such simulations to examine the finite time Lyapunov vectors and exponents. First, main results of “asymptotic” Lyapunov theory (based on Osseledec theorem²⁰) are summarized. Then, using a numerical simulation of two-dimensional turbulence, we highlight the different properties associated with finite time Lyapunov vectors and exponents, such as convergence in time and alignment properties. We also discuss the relations between the different categories of Lyapunov vectors. Finally, we examine the spatial distribution of FTLEs and the associated Lagrangian stirring.

II. LYAPUNOV THEORY

A. Tangent linear system

Lyapunov theory can be applied either directly to a material element vector advected in the flow or indirectly to the tracer gradient vector. Consider the equation of a Lagrangian trajectory,

$$\frac{D\mathbf{X}(t)}{Dt} = \mathbf{u}(\mathbf{X}(t), t),$$

where $\mathbf{X}(t)$ is the position of a particle at time t and $\mathbf{u}(\mathbf{X}(t), t)$ is its velocity at this time. The equation for the associated tangent linear system is simply

$$\frac{D\delta\mathbf{X}(t)}{Dt} = [\nabla\mathbf{u}(\mathbf{X}(t), t)]\delta\mathbf{X}(t),$$

where $\delta\mathbf{X}(t)$ stands for a material line element or the distance between two particles initially infinitesimally close. The matrix $[\nabla\mathbf{u}(\mathbf{X}(t), t)]$ is the velocity gradient tensor at the position $\mathbf{X}(t)$ at time t (hereafter we will drop the dependence on position and time). Now, consider the equation for a nondiffusive tracer q conserved along Lagrangian trajectories, i.e.,

$$\frac{Dq}{Dt} = \partial_t q + \mathbf{u} \cdot \nabla q = 0.$$

The tracer gradient ∇q satisfies

$$\frac{D\nabla q}{Dt} = -[\nabla\mathbf{u}]^\top \nabla q, \quad (1)$$

where $[\]^\top$ denotes the matrix transpose. It is easy to show that for an incompressible two-dimensional flow, the vector orthogonal to the tracer gradient $\mathbf{k} \times \nabla q$ (where \mathbf{k} denotes the unit vertical vector) satisfies the same equation as $\delta\mathbf{X}$. This is because $\nabla q \cdot \delta\mathbf{X} = \delta q$ is conserved as it is a tracer difference between two particles.²¹ Thus, in the rest of the paper, we will only use the tracer gradient vector.

Lyapunov theory introduces Lyapunov exponents and vectors which are associated, respectively, with the norm and the orientation of the tracer gradient. To introduce both quantities, we decompose the velocity gradient tensor in terms of vorticity ω , rate of strain σ , and orientation of the strain axes ϕ ,

$$[\nabla\mathbf{u}]^\top = \frac{1}{2} \begin{pmatrix} \sigma \sin 2\phi & \omega + \sigma \cos 2\phi \\ -\omega + \sigma \cos 2\phi & -\sigma \sin 2\phi \end{pmatrix}.$$

If we define the norm ρ and the orientation θ of the tracer gradient,

$$\nabla q = \rho (\cos \theta, \sin \theta),$$

the equations for θ and ρ are simply

$$2 \frac{D\theta}{Dt} = \omega - \sigma \cos 2(\theta + \phi), \quad (2a)$$

$$\frac{D \log \rho^2}{Dt} = -\sigma \sin 2(\theta + \phi). \quad (2b)$$

We also introduce the resolvent matrix of the system $M(t_1, t_2)$ which satisfies

$$\frac{D}{Dt} M(t_1, t) = [\nabla\mathbf{u}(\mathbf{X}(t), t)]^\top M(t_1, t)$$

with

$$M(t_1, t_1) = Id. \quad (3)$$

The matrix $M(t_1, t_2)$ is such that, for any gradient, $\nabla q(t_2) = M(t_1, t_2) \nabla q(t_1)$ and the square of the norm of the tracer gradient is related to the matrix $M(t_1, t_2)^\top M(t_1, t_2)$.

B. The Osseledec theorem

The Osseledec theorem²⁰ contains the essential results of the Lyapunov theory. Here we apply these general results to the tracer gradient problem in a two-dimensional flow (for a more general point of view, one can refer to the reviews by Eckmann and Ruelle²² and Legras and Vautard²³).

Consider a time integration of Eq. (1) between time t_1 and time t_2 (with $t_2 > t_1$) and suppose that $t_2 - t_1$ tends to infinity. The Osseledec theorem introduces a forward Lyapunov vector $F^+(t_1)$ and a Lyapunov exponent λ_∞ which satisfy the following properties.

(1) For any initial tracer gradient $\nabla q(t_1)$, with an orientation *different* from the forward Lyapunov vector $F^+(t_1)$, the tracer gradient grows exponentially at the rate λ_∞ over $[t_1, t_2]$, i.e.,

$$\lim_{t_2 - t_1 \rightarrow \infty} \frac{1}{t_2 - t_1} \log \frac{|\nabla q(t_2)|}{|\nabla q(t_1)|} = \lambda_\infty.$$

(2) If the initial tracer gradient is along $F^+(t_1)$, the tracer gradient will decay at the exponential rate $-\lambda_\infty$ over $[t_1, t_2]$.

The two Lyapunov exponents (λ_∞ and $-\lambda_\infty$) are of opposite sign because of the incompressibility of the flow. The forward Lyapunov vector $F^+(t_1)$ corresponds to the stable direction, i.e., the direction for which the tracer gradient norm is decaying in time. Another Lyapunov vector $G^+(t_1)$ can be introduced, such that $F^+(t_1)$ and $G^+(t_1)$ form an orthogonal basis of \mathbb{R}^2 . An important point of the Osseledec theorem is that the Lyapunov exponent λ_∞ is independent of particle positions whereas the vectors F^+ and G^+ depend on these positions at time t_1 .

We can also introduce a backward Lyapunov vector $F^-(t_2)$ at time t_2 with similar properties when considering a backward integration in time.

(1) For any initial tracer gradient $\nabla q(t_2)$, with an orientation different from the backward Lyapunov vector $F^-(t_2)$, the tracer gradient grows exponentially when integrating backward in time (i.e., from t_2 to t_1 , keeping $t_2 > t_1$).

(2) If the initial tracer gradient is along $F^-(t_2)$, the tracer gradient will decay at the exponential rate $-\lambda_\infty$ when integrating backward in time.

We also define the backward vector $G^-(t_2)$ as the vector orthogonal to $F^-(t_2)$. A consequence of the Osseledec theorem is that the backward vector $F^-(t_2)$ is linked to the behavior in the future, and the forward vector $F^+(t_1)$ to the behavior in the past.

(1) For any initial orientation of the tracer gradient at time t_1 , it will align with $F^-(t_2)$ at time t_2 , when $t_2 - t_1$ tends to infinity (i.e., when t_1 tends to $-\infty$).

(2) For any initial orientation of the tracer gradient at time t_2 , it will align with $F^+(t_1)$ at time t_1 for a backward integration, when $t_2 - t_1$ tends to infinity (i.e., when t_2 tends to $+\infty$).

The behavior of the tracer gradient thus depends not only on the Lyapunov exponent λ_∞ , but also on the vectors $F^-(t_2)$ and $F^+(t_1)$ as these vectors control the directions of decaying tracer gradients and the long-term behavior of their orientation.

C. Definition for finite times

Extending the results of the asymptotic theory to finite times is not straightforward because the evolution of the tracer gradient norm is strongly dependent on its initial orientation. However, the Osseledec theorem provides some guidance for introducing finite time Lyapunov exponents and vectors. The theorem states that the forward Lyapunov exponent λ_∞ and vectors (F^+ and G^+) are related to the asymptotic limit of the eigenvectors and eigenvalues of

$$U_\infty(t_1) = \lim_{t_2 - t_1 \rightarrow \infty} U(t_1, t_2)$$

where

$$U(t_1, t_2) = [M(t_1, t_2)^\top M(t_1, t_2)]^{1/[2(t_2 - t_1)]}. \quad (4)$$

More precisely, the eigenvalues of $U_\infty(t_1)$ are $\exp(\lambda_\infty)$ and $\exp(-\lambda_\infty)$ and their corresponding eigenvectors are $G^+(t_1)$ and $F^+(t_1)$. For finite times, the eigenvector of matrix $U(t_1, t_2)$ which corresponds to *maximum growth* over $[t_1, t_2]$ is often called the “singular vector” in predictability theory.²³ We will use the same terminology in what follows and we will denote it as g^+ . Its associated eigenvalue (or more exactly its logarithm) will be called the “singular value” (hereafter denoted λ_{FT}). The eigenvector g^+ of $U(t_1, t_2)$ converges toward $G^+(t_1)$ when $t_2 - t_1$ tends to infinity. In the same way, the eigenvector corresponding to the smallest eigenvalue (hereafter f^+) converges toward $F^+(t_1)$. A similar definition for g^- and f^- can be made for backward integration in time by using $U(t_2, t_1)$. This would define f^- as a “linear bred mode,” to keep the terminology of predictability theory,²³ meaning a mode which has already grown

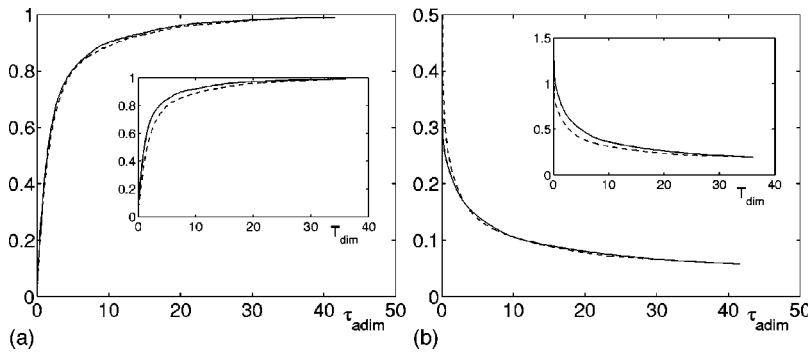
and equilibrated. Similarly, the finite time vector f^+ is also a “linear bred mode” since it has the same property but backward in time. The singular value λ_{FT} was introduced to define FTLEs by different authors^{24,25} and is in common use by the predictability community. However, it presents the disadvantage of being associated with a “singular” behavior as will be explained in Sec. VI.

III. NUMERICAL METHODS

In order to examine finite time Lyapunov properties, we use results from a numerical simulation at high resolution (1024^2) of freely decaying two-dimensional turbulence. We have computed the trajectories of 1024^2 particles initially on a regular grid at a time when vortices and vorticity filaments are present. The integration is made for 40 eddy turn-over times. Time is adimensioned by vorticity such that $\tau_{\text{adim}} = \int_{t_1}^{t_2} \langle \omega^2 \rangle^{1/2} dt$ where $\langle \omega^2 \rangle$ is the spatial average of enstrophy. A reason for this choice is that τ_{adim} is also the integral of the strain rate as $\langle \omega^2 \rangle = \langle \sigma^2 \rangle$ in two-dimensional turbulence. As discussed in Lapeyre *et al.*,^{15,16} the strain rate provides the time scale for the dynamics of the tracer gradient. The particle advection method is a fourth-order Runge–Kutta scheme with bicubic interpolation.²⁶ Along the Lagrangian trajectories, we integrate separately the equations of the tracer gradient orientation and the logarithm of its norm [i.e., Eqs. (2a) and (2b)]. This allows one to compute accurately both the norm and orientation of the tracer gradient since the logarithm of the norm grows only linearly with time. The integration of the tracer gradient equation is done off-line so that it is possible to do forward and backward integrations in time and test different initial orientations. The resolvent matrix M is computed by integrating two initially orthogonal tracer gradients. As a consistency check, we verified that the sum of the eigenvalues of U are zero at the numerical precision of the computer. Also, changing the initial condition of matrix M does not change the singular values, provided that the columns of $M(t_1, t_1)$ correspond to orthonormal vectors. As we use a Lagrangian method for integrating the tracer gradient equations, there is no real tracer and there is no small scale diffusion in the gradient equations, contrary to previous studies,^{16,17} so that the Lyapunov theory can be directly tested. The initial field is not the gradient of any tracer but this does not seem to be an issue in light of recent results on topological constraints of Lyapunov vectors.^{27,28} They demonstrated that the gradient nature of the field is recovered after a certain time and this implies that the asymptotic Lyapunov vectors and exponents are linked together by an equation involving spatial derivatives.

IV. CONVERGENCE IN TIME

Goldhirsh *et al.*²⁹ (see also Ershov and Potapov³⁰) showed that the convergence of the singular value toward the “asymptotic” Lyapunov exponent is rather slow (typically in t^{-1}) but the orientation of the singular vector converges more rapidly (typically exponentially in time) toward the Lyapunov vector $G^+(t_1)$. We can examine these convergence rates in our numerical simulation.



To estimate the convergence toward the Lyapunov vector, we use the fact that there are two different methods to compute the singular vector: first, the forward Lyapunov vector $G^+(t_1)$ corresponds to the asymptotic limit of the singular g^+ characterized by maximal growth over a finite time interval; second, random tracer gradients should align along the vector orthogonal to $G^+(t_1)$ [i.e., $F^+(t_1)$] when integrating backward in time. Thus, we compared the orientation $\theta_1(t_1)$ of g^+ with the orientation $\theta_2(t_1)$ of the vector orthogonal to a tracer gradient integrated backward in time with a random orientation at time t_2 . Figure 1(a) presents the average cosine of $2(\theta_1 - \theta_2)$ as a function of the adimensional integration time $\tau_{\text{adim}} = \int_{t_1}^{t_2} \sigma_{\text{rms}} dt$ (keeping fixed either t_1 or t_2). We observe a rapid convergence and a correlation of 0.95 is reached after 20 eddy turn-over times. Moreover the correlations for backward and forward integrations are overlapping, which means that the process is essentially the same for both integrations in time and that τ_{adim} captures its time scale [compare with the inset of Fig. 1(a)] which shows the same quantities as a function of $T_{\text{dim}} = t_2 - t_1$.

Concerning the Lyapunov exponent convergence, each particle in the flow should converge to the same Lyapunov exponent λ_∞ . However in decaying turbulence, all quantities (vorticity, strain rate, etc.) are slowly decaying following a power law and the asymptotic Lyapunov exponent should be exactly zero. It is thus more interesting to compute the time evolution of the standard deviation of the finite time Lyapunov exponent $\langle (\lambda_{\text{FT}}(\mathbf{x}) - \langle \lambda_{\text{FT}}(\mathbf{x}) \rangle)^2 \rangle^{1/2}$ as a function of τ_{adim} . As we can see from Fig. 1(b), the standard deviations of the backward and forward FTLEs decay slowly in time, which contrasts with the fast convergence of the Lyapunov vectors. The decay rate is different for the backward and forward exponents [see the inset of Fig. 1(b)] because the turbulence is decaying in time so that the stirring processes are more efficient at time t_1 than at time t_2 (with $t_2 > t_1$). To nondimensionalize the main plots of Fig. 1, we have used τ_{adim} as the Lyapunov exponent is the inverse of a time scale. Some differences still exist for small times because of the realignment of the singular vectors toward their asymptotic vectors.

Concerning the evolution of the Lyapunov exponents toward their asymptotic values, the probability density function (pdf) of the Lyapunov exponent (Fig. 2) shows two processes occurring at the same time: first, there is a narrowing of the pdf as a function of time, corresponding to the slow

FIG. 1. (a) Average cosine of twice the angle difference of finite time Lyapunov vectors computed by two different methods as a function of adimensional time τ_{adim} (see the text for an explanation). Continuous curve: for $g^+(t_1)$. Dashed curve for $g^-(t_2)$. In the inset, the same quantities are plotted, but as a function of dimensional time. (b) Adimensional standard deviation of Lyapunov exponent λ_{FT} as a function of time. Continuous curve: forward integration. Dashed curve: backward integration. In the inset, the same quantities are plotted, but in dimensional units.

decrease of the standard deviation discussed above. This is consistent with theory and with results on FTLE probability density functions in chaotic flows and in forced turbulence.^{21,31} Second, we observe a shift of the peak of the pdf toward smaller values as the turbulence is decaying in time. However we can anticipate that the narrowing rate of the pdf toward its mean value should depend also on the magnitude of the stirring processes and the narrowing rate would decrease as time increases. The processes of homogenization of the FTLEs (associated with the narrowing of the pdf) and of decay of the exponents are thus competing and the homogenization occurs first in our simulation because the turbulence is slowly decaying. If the decay were faster, we would expect the homogenization to be weaker and different regions of the turbulence would have different long-term Lyapunov exponents.

The slow convergence of the exponent toward its mean value is related to the reorientation of the tracer gradient toward its “equilibrium” orientation. Actually, the singular value can be expressed as the time average of the instantaneous exponential growth rate of the tracer gradient by

$$\lambda_\infty = \lim_{t_2 - t_1 \rightarrow \infty} \frac{1}{t_2 - t_1} \int_{t_1}^{t_2} \frac{D \log |\nabla q(t)|}{Dt} dt.$$

The instantaneous exponential growth rate of the tracer gradient depends only on the orientation of the gradient (and not on its norm) as seen in Eq. (2b). Because of the rapid convergence of the orientation toward the Lyapunov vector, we

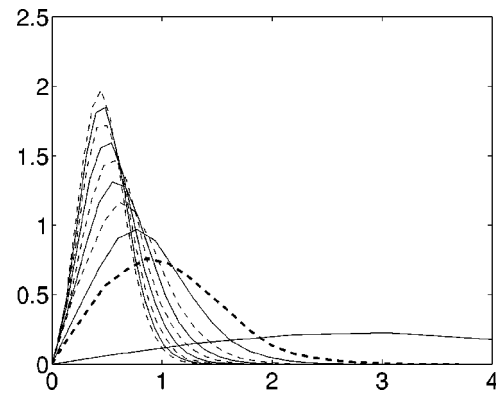


FIG. 2. PDF of the Lyapunov exponent for different times. As time increases, the pdf is narrowing and the peak is increasing and shifting toward smaller values. The pdfs are plotted every $\tau_{\text{adim}} = 5$. The dashed and bold curve corresponds to a total time $\tau_{\text{adim}} = 6$.

can assume that after a time $t_{1/2}$, the tracer gradient is “equilibrated” (i.e., dependent only on the flow properties and not on its initial orientation) through the rest of the time. This implies that the tracer gradient growth rate will be independent of the initial condition after time $t_{1/2}$ and will be equal to the growth rate associated with the Lyapunov vector. Thus the difference in orientation between the Lyapunov vector and the singular vector over $[t_1, t_{1/2}]$ transforms into an error of the form

$$\frac{1}{t_2 - t_1} \int_{t_1}^{t_{1/2}} (\) dt.$$

When t_2 tends to infinity, this is proportional to $(t_2 - t_1)^{-1}$, which gives the slow convergence rate for the singular value.

V. ALIGNMENT PROPERTIES

The Osseledec theorem states that a tracer gradient initially in a “random” orientation at time t_1 will align with the backward Lyapunov vector $F^-(t_2)$ at time $t_2 > t_1$ when $t_2 - t_1$ is large. This proves that for each time t_2 there is a natural tendency for the tracer gradient vector to align in a certain orientation independent of its initial orientation. This is also true for an integration backward in time: the tracer gradient will align along $F^+(t_1)$ when integrating from $t_2 > t_1$. As shown in Sec. IV, this convergence is very fast indeed (exponentially in time) and contrasts with the slow convergence of the FTLE. This proves that more emphasis should be put on the dynamics of the tracer gradient orientation. The rapid convergence allows one to use an assumption of stationarity for the velocity gradient tensor (or its derivatives) as was done in different studies.^{16,17,32–34} In particular, the assumption of a slowly varying velocity gradient tensor in the strain basis (what we call an “adiabatic approximation”) is able to highlight the mechanisms of the tracer gradient dynamics.^{16,17} The strain basis is formed by the eigenvectors of the strain matrix (i.e., $\frac{1}{2}([\nabla \mathbf{u}] + [\nabla \mathbf{u}]^\top)$). In the strain basis (formed by the eigenvectors of the strain matrix $\frac{1}{2}([\nabla \mathbf{u}] + [\nabla \mathbf{u}]^\top)$), the equation of the orientation of the tracer gradient simplifies to

$$\frac{D\zeta}{Dt} = \sigma (r - \cos \zeta), \quad (5)$$

where $\zeta = 2(\theta + \phi)$. The quantity $r = (\omega + 2(D\phi/Dt))/\sigma$ is the ratio between the effect of effective rotation (due to vorticity in the strain basis) and the effect of strain. Assuming a slow variation in time of the quantity r and in regions dominated by strain (where $|r| \leq 1$), the tracer gradient should align with an orientation $\zeta_- = -\arccos r$ corresponding to the stable fixed point of Eq. (5) as shown by Lapeyre *et al.*¹⁶ In regions dominated by “effective rotation” (where $|r| > 1$), the tracer gradient is rotating but the rotation rate is variable in time so that another parameter is involved in the dynamics. This parameter is $s = [D(\sigma^{-1})]/Dt$ and corresponds to the evolution of the time scale of the dynamics (σ^{-1}). In these regions, the orientation ζ aligns with an orientation $\alpha = \arctan(s/r) + \pi(1 - \text{sign}(r))/2$ as was observed by Klein *et al.*¹⁷ An interesting feature is that the quantities r and s are invariant under solid body rotation, keeping the same invari-

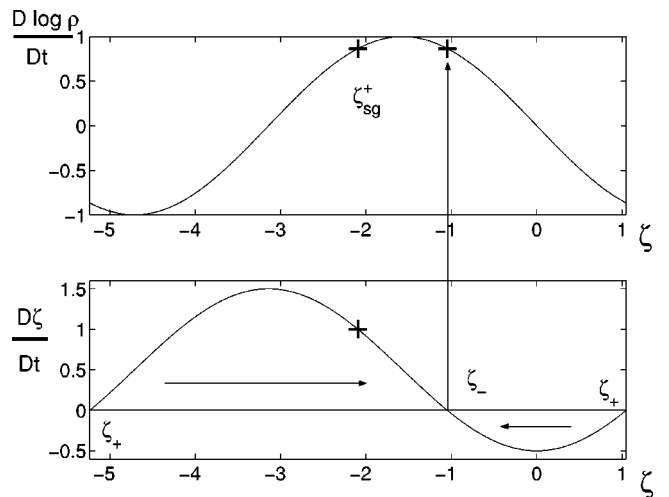


FIG. 3. Top: $(D \log \rho / Dt)$ as a function of ζ . Bottom: $D\zeta / Dt$ as a function of ζ for $r=0.5$. The horizontal arrows symbolize the evolution of ζ . The crosses correspond to ζ_{sg}^+ and ζ_- . ζ_+ is indicated twice because it is defined modulo 2π .

ance as the tracer gradient equation. This is because the “effective rotation” in the numerator of r is the difference between rotation due to vorticity and strain axis rotation. (The angle between the compressional strain axis and the x axis is $-\phi - \pi/4$, so $D\phi/Dt$ is of opposite sign of the strain axis rotation.) Relating this alignment tendency with the Lyapunov theory, we see that the orientation $\zeta_{eq}^-(t_2)$ defined by

$$\zeta_{eq}^- = \begin{cases} -\arccos r & \text{where } |r| \leq 1 \\ \arctan\left(\frac{s}{r}\right) + \frac{\pi}{2}(1 - \text{sign}(r)) & \text{where } |r| > 1, \end{cases}$$

is in fact an estimate of the orientation of backward Lyapunov vector $F^-(t_2)$. Similarly, the orientation $\zeta_{eq}^+(t_2)$ defined by

$$\zeta_{eq}^+ = \begin{cases} \arccos r & \text{where } |r| \leq 1 \\ \arctan\left(\frac{s}{r}\right) + \frac{\pi}{2}(1 - \text{sign}(r)) & \text{where } |r| > 1, \end{cases}$$

is an estimate of the orientation of the forward Lyapunov vector $F^+(t_1)$ in the same approximation.

The adiabatic approximation used to derive ζ_{eq}^\pm can also provide an estimate of the singular vectors. In the regime dominated by strain ($|r| \leq 1$), we can prove that the orientation of maximum growth corresponds to $\zeta_{sg}^+ = \pi + \arccos r$ when considering long times (i.e., such that $\int_{t_1}^{t_2} \sigma dt \gg 1$). To demonstrate this point, we can examine the instantaneous tracer gradient growth rate (upper part of Fig. 3) and the Lagrangian time derivative of ζ (lower part of Fig. 3) as functions of ζ . We see that the fixed point ζ_- is not associated with the largest possible growth (which corresponds to $\zeta = -\pi/2$). For an initial orientation $\zeta(t=0)$ of the tracer gradient along ζ_{sg}^+ (which has the same growth rate initially as ζ_-), its growth rate is always larger than the one corresponding to ζ_- . Examining the other possible initial conditions (either in $[\zeta_-, \zeta_+]$, $[\zeta_{sg}^+, \zeta_-]$ or $[\zeta_+, \zeta_{sg}^+]$), we see that

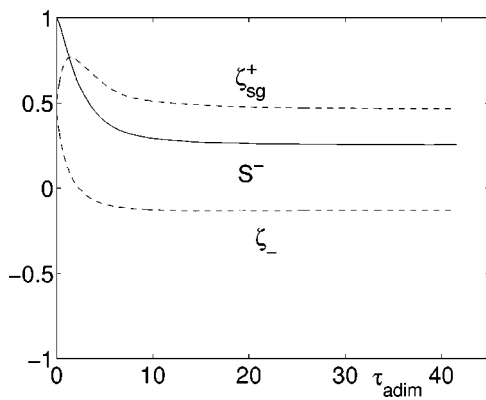


FIG. 4. Average cosine between forward singular vector g^+ and adiabatic approximation ζ_{sg}^+ , compressional strain eigenvector S^- and adiabatic equilibrium solution ζ_- as a function of adimensional time τ_{adim} .

the time interval can be split into two parts: one for which the growth rate will be smaller than for the tracer gradient initially along ζ_{sg}^+ ; and another one for which it will have the same behavior as the latter orientation. This argument proves that the orientation ζ_{sg}^+ should be an estimate of the Lyapunov vector G^+ if the adiabatic approximation is valid. Similarly, we expect $\zeta_{\text{sg}}^- = \pi - \arccos r$ to be a good approximation of the backward singular vector in regions where $|r| < 1$. To extend this results to regions dominated by the “effective rotation,” we can use the orthogonality of F^+ and G^+ (or F^- and G^-) so that ζ_{sg}^\pm should be equal to $\pi + \zeta_{\text{eq}}^\pm$, i.e.,

$$\zeta_{\text{sg}}^\pm = \begin{cases} \pi \pm \arccos r & \text{where } |r| \leq 1 \\ \arctan\left(\frac{s}{r}\right) + \frac{\pi}{2}(3 - \text{sign}(r)) & \text{where } |r| > 1. \end{cases}$$

This last equality uses the notion of biorthogonality of Farrell and Ionnaou.²⁴

To examine these estimates in the numerical simulation, we computed the cosine of twice the relative angle of the forward singular vector g^+ with different orientations as a function of the adimensional time τ_{adim} (Fig. 4). These orientations are the compressional strain axis S^- (corresponding to $\zeta = -\pi/2$) and the adiabatic solutions ζ_{eq}^- and ζ_{sg}^+ , all of these computed at time t_1 . Initially, we observe the singular vector g^+ to be in the direction of S^- . This is an exact result since $(D/Dt)(M^T M)(t_1, t_1) = 2S$, and in an expansion at a first order in time, $M^T M = Id + 2tS + O(t^2)$. The alignment with the strain eigenvector decreases rapidly in time and after 10 adimensional time units, the average cosine is only 0.3. During the same period, the average cosine of the adiabatic approximation of the singular vector increases to reach a maximum of 0.8 at about 2 time units and then decreases around 0.5. This demonstrates that our assumption of stationarity for the quantity r (i.e., the adiabatic approximation) seems strictly valid for a few turn-over times but the estimated ζ_{sg}^+ direction gives a good estimate of the true singular vector even for long times. Actually a direct computation of the mean adimensional time of validity of the adiabatic assumption (not shown) shows that this time is larger than one turn-over time for 30% of particles and this is even

greater (40%) in regions dominated by strain (where $|r| < 1$). Concerning the backward integration in time, an identical evolution is observed (not shown) but the roles are changed: initially the backward singular vector g^- is aligned with S^+ (corresponding to $\zeta = +\pi/2$), then it aligned with ζ_{sg}^- whereas the correlation with ζ_{eq}^+ remains small.

Since $F^+(t_1)$ and $G^+(t_1)$ are orthogonal and since ζ_{eq}^+ and ζ_{sg}^+ are also orthogonal, the alignment between the forward vector F^+ and $\zeta_{\text{eq}}^+(t_1)$ is exactly equivalent to the alignment between ζ_{sg}^+ and the forward vector G^+ . Thus, Fig. 4 shows that $\zeta_{\text{eq}}^+(t_1)$ well approximates the forward Lyapunov vector $F^+(t_1)$. Similarly, $\zeta_{\text{eq}}^-(t_2)$ well approximates the backward Lyapunov vector $F^-(t_2)$ (not shown), which is consistent with our previous results.^{16,17}

VI. DIFFERENCES BETWEEN LYAPUNOV VECTORS

A. Singular vectors versus bred modes

In the preceding discussion, two classes of Lyapunov vectors were introduced: the “bred modes” associated with alignment of the tracer gradient after equilibration [$f^-(t_2)$ and $f^+(t_1)$ for backward and forward integrations in time] and the singular vectors associated with maximal tracer gradient growth over a finite time interval [$g^-(t_2)$ and $g^+(t_1)$]. We can use the adiabatic solutions to gain some insights into the differences between these vectors.

As was shown by the dynamical argument in Sec. V, the orientations ζ_{sg}^\pm are not at all related to an equilibrium: they are associated with a kinematic effect in the sense that growth rate and orientation properties are out of phase, so that the equilibrium orientations ζ_{eq}^\pm do not correspond to the largest possible growth rate. This is observed in the numerical simulation (Fig. 4) since the correlation of ζ_{eq}^- with g^+ is very weak whereas it is stronger for ζ_{sg}^\pm . Moreover the correlation of g^+ with f^- presents the same tendency as the correlation with ζ_{eq}^- (not shown). This behavior is related to the non-normality of $\nabla \mathbf{u}$ (expressed in the strain basis), i.e., the fact that $\nabla \mathbf{u}$ has nonorthogonal eigenvectors.²⁴ Two limiting cases can highlight these differences. In a pure strain field (for which $r=0$), the orientations ζ_{sg}^+ and ζ_{eq}^- are equal, which means that the tracer gradient converges toward the vector corresponding to the largest growth rate (the compressional strain axis here). In this case, the equation of the norm and of the orientation of the gradient are in phase and the velocity gradient in the strain basis has orthogonal eigenvectors. For an axisymmetric vortex, the situation is quite different since r equals ± 1 (see Lapeyre *et al.*¹⁶) and the orientations ζ_{eq}^- and ζ_{sg}^+ are now orthogonal. In this case, the tracer gradient at equilibrium is orthoradial whereas the largest growth over a finite time can be obtained when the gradient is oriented in the radial direction. It is interesting to note that these two orientations correspond to no instantaneous growth of the tracer gradient. This behavior indicates the importance of the rotation due to the vorticity in the strain basis (what we call the “effective rotation”) in driving the non-normality of the operator. The competition between effective rotation and strain is the main mechanism that drives the difference between ζ_{eq}^- and ζ_{sg}^+ and seems also to explain the difference between F^- and G^+ in the numeri-

cal simulation. The orientations g^\pm (and G^\pm) are therefore not instructive *per se* to understand the dynamics associated with Lyapunov theory. They correspond to the “extreme” behavior for the tracer gradient whereas the Lyapunov vectors F^\pm correspond to the equilibrated (or “mean”) behavior.

B. Backward versus forward vectors

There also exists a distinction between forward and backward Lyapunov vectors. The Osseledec theorem shows that these vectors are associated with different properties for forward and backward integration in time but these properties are not directly comparable.

Again we can use the adiabatic approximation to emphasize the differences. In the case of a pure strain field ($r=0$), the backward orientation ζ_{eq}^- and the forward orientation ζ_{eq}^+ are orthogonal corresponding to the compressional and extensional strain axes. In this situation, they correspond to orientations of growth for the tracer gradient, either in backward or forward integration in time. For the more general case $|r|<1$, the equilibrium orientations ζ_{eq}^\pm are different and also correspond to growth of the tracer gradient integrated forward or backward in time. On the other hand, for an axisymmetric vortex, the two orientations ζ_{eq}^\pm are equal. For the more general case of $|r|>1$, ζ_{eq}^\pm are also equal but the forward growth rate $(D/Dt) \log|\nabla q| = -\sigma \sin \zeta_{\text{eq}}^- = -\sigma s/\sqrt{r^2+s^2}$ is strictly opposite to the backward growth rate $-(D/Dt) \log|\nabla q| = \sigma \sin \zeta_{\text{eq}}^+ = \sigma s/\sqrt{r^2+s^2}$ (as time is reversed). This is because a growth in a forward integration corresponds to a decay in a backward integration in this rotation regime.

The difference between ζ_{eq}^- and ζ_{eq}^+ relates to the reversibility or irreversibility of the tracer gradient dynamics. So we can interpret the difference between the Lyapunov vectors F^- and F^+ to be a consequence of local reversibility or irreversibility of the flow (of course, if a trajectory passes from a region with chaotic behavior to a region with reversible behavior, it is globally chaotic). To diagnose such a behavior we can compare the instantaneous growth rate of the tracer gradient at time t when integrated from the past (i.e., from time t_1 such that $t-t_1>0$ is large) with the growth rate at time t when integrated from the future (i.e., from time t_2 such that t_2-t is large). This corresponds to comparing $(D/Dt) \log|\nabla q|$ for an orientation along $F^-(t)$ and $-(D/Dt) \log|\nabla q|$ for an orientation along $F^+(t)$ [Eckhardt and Yao³⁵ introduced the growth rate along $F^-(t)$ to measure a local Lyapunov exponent for a different purpose]. Figure 5 presents the joint probability density function of these two quantities computed after a time integration such that $\int_{t_1}^t \sigma_{\text{rms}} dt = \int_t^{t_2} \sigma_{\text{rms}} dt = 20$. As expected, we observe two different regimes: a regime along the anti-bisector corresponding to opposite growth rates. This means that in these regions, the dynamics is instantaneously nonchaotic, and the behavior of the gradients is reversible. The second regime corresponds to the large branch along the bisection in the positive quadrant corresponding to growths forward and backward in time. These regions are associated with strong irreversibility of the system, since if we integrate forward

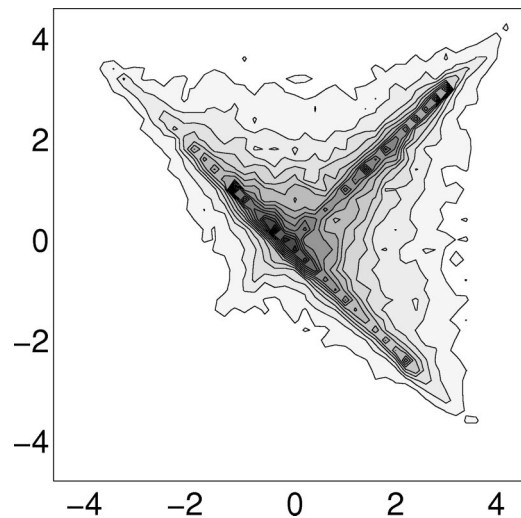


FIG. 5. Joint PDF of the forward and backward growth rates computed, respectively, with an orientation along F^- and F^+ .

and backward the tracer gradient equations along the same trajectory, we will obtain a different solution than the initial condition.

We tried to relate the two regimes to the quantity r and found that the regions of irreversibility are well correlated with $|r|<1$ whereas the regions more predictable are correlated with $|r|>1$ (not shown). The numerical simulation thus confirms the prediction of the adiabatic approximation and shows that forward and backward Lyapunov vectors tend to have same sign or opposite sign growth rates but with the same amplitude. This could explain why stable and unstable invariant manifolds often display the same orientation (as should be the case in regions dominated by “effective rotation”) whereas they intersect near hyperbolic points (as they correspond to different or even orthogonal orientations as should be the case in regions dominated by strain).

VII. SPATIAL DISTRIBUTION OF FTLEs

There have been numerous studies of finite time Lyapunov exponents in two dimensions but most of them concentrated on the statistics of the Lyapunov exponents in relation to the tracer field.^{31,36–38} Some of them examined the spatial distribution of the Lyapunov exponents in a two-dimensional chaotic flow.^{8,25} To our knowledge, we give here the first description of the spatial distribution of FTLE in freely decaying turbulence. Only Babiano *et al.*³⁹ examined some particular trajectories for this type of flow.

The time evolution of the spatial distribution of Lyapunov exponents is very similar in our turbulent simulations to that found by Pierrehumbert and Yang⁸ in their calculation for the troposphere: for small time integration, large FTLEs (Fig. 5) concentrate in patches with shapes identical to the distribution of the strain rate (not shown). This is because the strain rate controls the short-term behavior of the singular value as explained in Sec. V. Then, these patches become thinner and thinner and transform into filaments of large FTLEs (see Fig. 6). As time proceeds, these filaments become narrower and fill the background flow but their

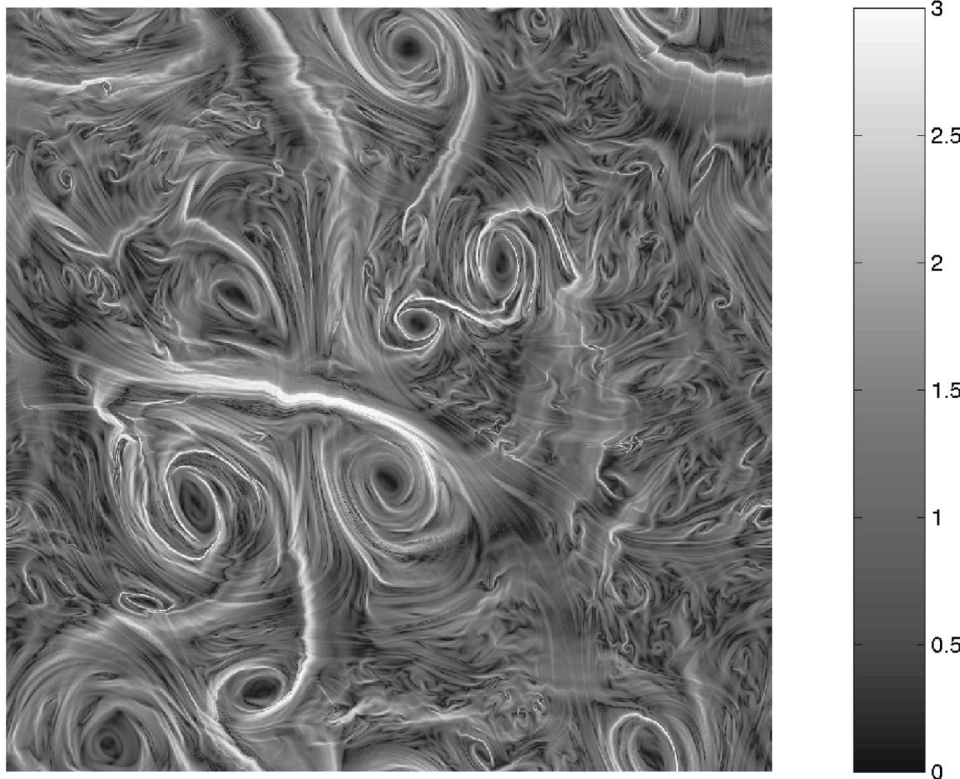


FIG. 6. Finite time Lyapunov exponent for $\tau_{\text{adim}}=6$, plotted at initial positions.

Lyapunov exponents decrease and tend to the spatial mean value as particles are experiencing different straining regions (not shown). This process shows that spatial homogenization of the Lyapunov exponent proceeds rapidly as particles have time to wander through the flow. Then, the Lyapunov exponent of the particles will slowly decay as the turbulence is also decaying. Finally, the FTLE field will tend to the value $\lambda_\infty=0$. Figure 6 displays the FTLE after a time $\tau_{\text{adim}}=6$ (the most interesting stage in our opinion) corresponding to the presence of filaments with large values of the Lyapunov exponents (compared with the spatial mean exponent $\langle \lambda \rangle \approx 1$). For reference, the pdf of FTLEs corresponds to the bold and dashed curve in Fig. 2. The filaments present in the figure could be the signature of the invariant manifolds in the turbulent flow field.

Concerning the spatial distribution of the FTLEs, three different categories of structures can be described. There are large scale filaments that correspond to the largest exponents. These filaments start from the neighborhood of one vortex and end close to the vicinity of another vortex (see, for instance, the long and horizontal filament in the center of Fig. 6). They are associated with the *interaction of vortices* which leads to a large straining. This can be demonstrated by examining the Lyapunov exponent at the *final* positions of particles at t_2 (Fig. 7) (actually this figure represents the norm of the gradient of a real tracer during the stage where diffusion does not play any role). The very long filament starting from the top of Fig. 7 and ending at the bottom near the asymmetric dipole corresponds to the horizontal filament with large FTLE on Fig. 6. As trajectories indicate (not shown), the formation of the dipole of the bottom center of Fig. 7 leads to the ejection of material and to this very long filament. The

same process occurs with the two vortices at the bottom right- and left-hand corners of Fig. 6, which are responsible for the filament at the top right-hand corner of Fig. 6 and which lead to the dipole at the bottom right- and left-hand corners of Fig. 7 (remember that the domain is doubly periodic). A last example corresponds to the vortex at the top center of Fig. 6: a filament starts from this vortex and ends up near the two smaller vortices close to the center of the figure. In Fig. 7, we see that these three vortices at the top center of the figure are very close at this time, leading to a very strong straining. These FTLEs that start from the vicinity of one vortex and terminate at the vicinity of another one are due to the future interactions of these vortices that provide the straining and nonlocal transport associated with it.

Another kind of structure corresponds to the filaments that wind up around the vortices in spirals. This is generally the case for vortices that are close to axisymmetric shape (for instance the vortex at the center of Fig. 6). These filaments are associated with ejection of material from inside the vortex to its surroundings, thus they materialize the transport *in the vicinity of the vortex*. They are densely packed around vortices and the vortex core is characterized by low values of Lyapunov exponents, consistent with Babiano *et al.*³⁹ Particles seeded uniformly in a box around the vortex (Fig. 8) tend to stay in the vicinity of the vortex even if their Lyapunov exponent is high. Some particles even enter the vicinity by the interplay of the large scale filament. The vortex core is well defined as particles do not generally leave the core and have low FTLEs (see the particles in gray in Fig. 8). We therefore speculate that the layered structure of FTLE around the circular vortices is just the “circulating cell” described by Elhmadi *et al.*² or the “stochastic layer” dis-

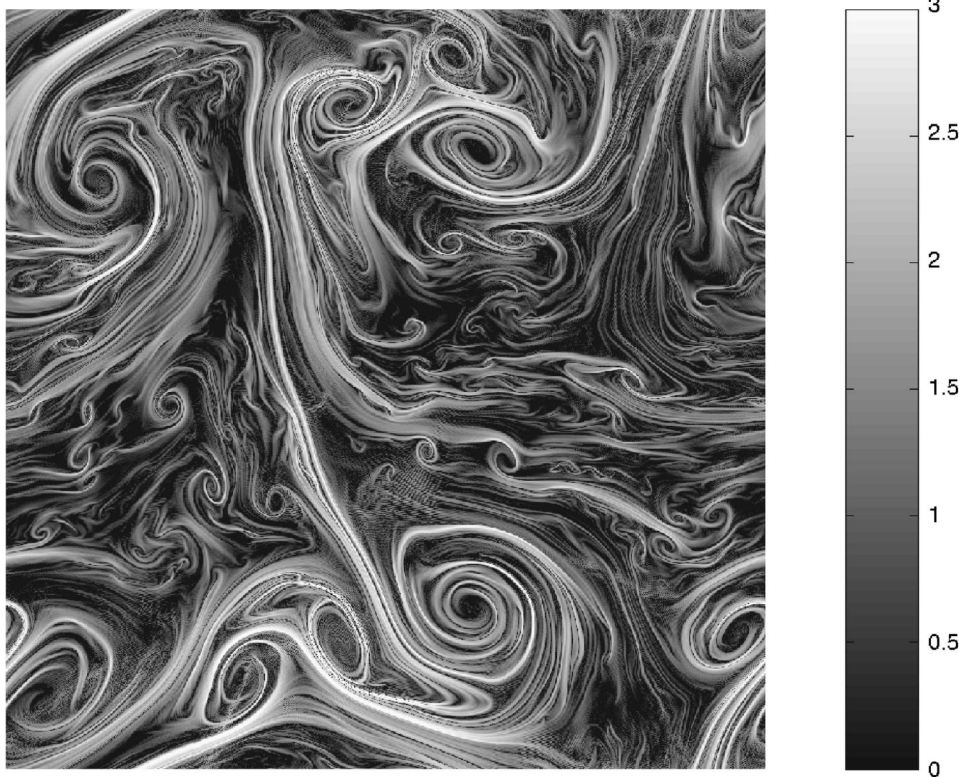


FIG. 7. Finite time Lyapunov exponent for $\tau_{\text{adim}}=6$, plotted at final positions.

cussed by Joseph and Legras.¹⁴ This region controls the exchange between the far field and the interior of the vortex: a particle that exits a vortex core is trapped for a very long time in that region before it is expelled to the far field. It is interesting to note that elliptical vortices have a few filaments that wind up around them, and their edges (i.e., their circulating cell) seem thinner. These elliptical vortices have a geometrical structure very similar to the Kida vortex^{15,40} with two long filaments surrounding the vortex and extending to the far field. This circulating cell around the vortices could act as a dynamical barrier: a circular shape is associated with a thick stochastic layer that prevents mixing between the vortex core and the far field whereas an elliptical shape is associated with a thinner layer and the interior of the vortex can be mixed more easily with the far field.

A last category of structures corresponds to low values of Lyapunov exponents in the background turbulent field. It is associated with low values of the strain rate and corresponds to vortices of smaller and smaller scale and amplitude but with properties analogous to the large scale vortices.

Finally, the distribution of FTLEs shows the intricacy of chaotic mixing in two-dimensional turbulence: the properties of mixing depend not only on the shape of the vortices and their stochastic layer but also on the nonlocal interaction that allows mixing to spread from the vicinity of one vortex to another one. The FTLE with largest values are the signature of the future interactions between coherent structures.

VIII. CONCLUSION

We have discussed the link between recent results on tracer gradient dynamics and Lyapunov theory using a numerical simulation of two-dimensional turbulence to illus-

trate our points. Lyapunov theory predicts not only the time evolution of the norm of the tracer gradient but more importantly the existence of orientations toward which the tracer gradient converges. The rapid convergence of the orientation contrasts with the slow convergence of the Lyapunov exponent and justifies the importance of the dynamics of the orientation. Two types of structures emerge from Lyapunov theory: singular vectors g^\pm associated with maximum tracer gradient growth over a finite time and “linear bred mode” vectors F^\pm toward which tracer gradients align. These two types are intrinsically different because the first one is associated with extreme behavior and the other one with equilibrium (or “mean”) behavior of the tracer gradient. This difference is due to the importance of strain for the singular vectors and effective rotation for stable Lyapunov vectors as the numerical simulations confirms it. Moreover, these orientations can be estimated from local velocity and acceleration gradient tensors by the so-called “adiabatic approximation.”^{16,17} Another point is that the relative orientations of forward and backward Lyapunov vectors allow one to determine the local “irreversibility” of the tracer gradient dynamics.

We also examined the spatial distribution of finite time Lyapunov exponents in the two-dimensional flow field. The FTLEs present an intricate structure which strongly depends on the shape of the vortices for local transport (i.e., in the vicinity of the vortex): nearly circular vortices have a broad circulating cell which seems to prevent mixing between the far field and the interior of the vortex whereas elliptical vortices have a narrow circulating cell. Some large scale filaments of large values of FTLE are also present because of

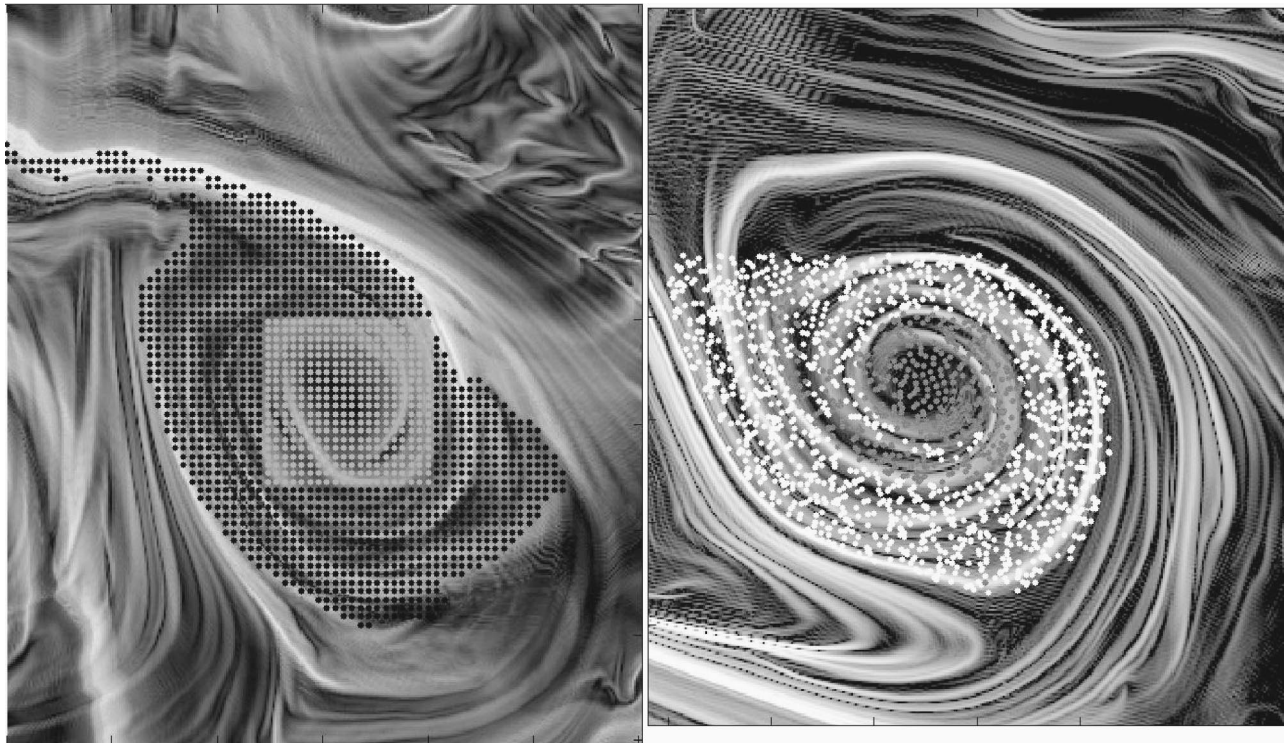


FIG. 8. Initial (left) and final (right) positions of particles seeded near the circular vortex of Fig. 6.

the interaction between vortices and govern the nonlocal transport properties.

Finally, this paper tried to clarify what Lyapunov theory can teach us for the properties of chaotic advection by two-dimensional flows. The Lyapunov approach was used in many studies but with different points of view. The Okubo³²–Weiss³³ (OW) criterion and the Hua and Klein (HK)³⁴ criterion were introduced to understand the instantaneous dynamics of the tracer gradient related to *local* growth or rotation of the gradient. However, these criteria are not directly related to Lyapunov exponents as the Lyapunov exponents correspond to a tracer gradient growth rate averaged along a Lagrangian trajectory, which is *nonlocal* by nature. This explains why finite time Lyapunov exponents give very different results from OW and HK criteria as illustrated by Boffetta *et al.*⁴¹ The Okubo–Weiss and Hua and Klein approaches were indeed relevant for the dynamics of the orientation of the Lyapunov vectors as the dynamics is decomposed by these criteria in terms of the competition of rotation and strain. This competition drives the dynamics of the orientation of the tracer gradient (see Lapeyre *et al.*,¹⁶ Klein *et al.*,¹⁷ and Sec. V of the present paper). To recover the Lyapunov exponent, one then needs to integrate the information of the dynamics of the orientation along Lagrangian trajectories through the tracer gradient growth rate. This is basically the approach followed by Lapeyre *et al.*¹⁵ This kind of approach for studying transport barriers or invariant manifolds is preferable than directly diagnosing finite time Lyapunov exponents because of the slow convergence of the FTLE as shown by Boffetta *et al.*⁴¹ for a nontrivial test case. Other alternative approaches exist, such as the method of Haller^{13,42} to diagnose invariant manifolds, the finite size

Lyapunov exponent technique,^{9,41} or effective diffusivity.^{43,44} These methods give good results because of their fast convergence in time but their basic properties are not yet well understood.

ACKNOWLEDGMENTS

This work was initiated in Laboratoire de Physique des Océans (France). The numerical simulations were performed at IDRIS (CNRS), Orsay, France. During the writing of the paper, I was supported by the Visiting Scientist Program in Atmospheric and Oceanic Sciences at Princeton University. I am grateful for numerous thoughtful suggestions from Lien Hua and Patrice Klein. Discussions with Bernard Legras on the concept of dynamical barrier are also acknowledged. Brian Arbic improved the manuscript with his comments.

¹R. T. Pierrehumbert, “Chaotic mixing of tracer and vorticity by modulated travelling Rossby waves,” *Geophys. Astrophys. Fluid Dyn.* **58**, 285 (1991).

²D. Elhmaïdi, A. Provenzale, and A. Babiano, “Elementary topology of two-dimensional turbulence from a Lagrangian viewpoint and single-particle dispersion,” *J. Fluid Mech.* **257**, 533 (1993).

³Z. Neufeld and T. Tél, “Advection in chaotically time-dependent open flows,” *Phys. Rev. E* **57**, 2832 (1998).

⁴A. Provenzale, “Transport by coherent barotropic vortices,” *Annu. Rev. Fluid Mech.* **31**, 55 (1999).

⁵T. Tél, G. Karolyi, A. Péntek, I. Scheuring, Z. Toroczkai, C. Grebogi, and J. Kadtke, “Chaotic advection, diffusion, and reaction in open flows,” *Chaos* **10**, 89 (2000).

⁶H. Aref, “Stirring by chaotic advection,” *J. Fluid Mech.* **143**, 1 (1984).

⁷J. M. Ottino, *The Kinematics of Mixing: Stretching, Chaos and Transport* (Cambridge University Press, Cambridge, 1989).

⁸R. T. Pierrehumbert and H. Yang, “Global chaotic mixing on isentropic surfaces,” *J. Atmos. Sci.* **50**, 2462 (1993).

⁹V. Artale, G. Boffetta, A. Celani, M. Cencini, and A. Vulpiani, “Disper-

- sion of passive tracers in closed basins: Beyond the diffusion coefficient," *Phys. Fluids* **9**, 3162 (1997).
- ¹⁰J. Guckenheimer and P. Holmes, *Nonlinear Oscillations, Dynamical Systems, and Bifurcations of Vector Fields* (Springer, New York, 1983).
- ¹¹S. Wiggins, *Chaotic Transport in Dynamical System* (Springer, New York, 1992).
- ¹²N. Malhotra and S. Wiggins, "Geometric structures, lobe dynamics and Lagrangian transport in flows with aperiodic time dependence, with applications to Rossby wave flow," *J. Nonlinear Sci.* **8**, 401 (1998).
- ¹³G. Haller, "Finding invariant manifolds in two-dimensional velocity fields," *Chaos* **10**, 99 (2000).
- ¹⁴B. Joseph and B. Legras, "Relation between kinematic boundaries, stirring and barriers for the Antarctic polar vortex," *J. Atmos. Sci.* **59**, 1198 (2002).
- ¹⁵G. Lapeyre, B. L. Hua, and B. Legras, "Comments on 'Finding finite-time invariant manifolds in two-dimensional velocity fields,'" *Chaos* **11**, 427 (2001).
- ¹⁶G. Lapeyre, P. Klein, and B. L. Hua, "Does the tracer gradient vector align with the strain eigenvectors in 2-D turbulence?" *Phys. Fluids* **11**, 3729 (1999).
- ¹⁷P. Klein, B. L. Hua, and G. Lapeyre, "Alignment of tracer gradient vectors in 2D turbulence," *Physica D* **146**, 246 (2000).
- ¹⁸A. Adrover and M. Giona, "Measure-theoretical properties of the unstable foliation of two-dimensional differentiable area-preserving systems," *Phys. Rev. E* **60**, 347 (1999).
- ¹⁹G. Haller, "Lagrangian structures and the rate of strain in a partition of two-dimensional turbulence," *Phys. Fluids* **13**, 3365 (2001).
- ²⁰V. Osseledec, "A multiplicative ergodic theorem. Lyapunov characteristic numbers for dynamical systems," *Trans. Moscow Math. Soc.* **19**, 197 (1968).
- ²¹F. Városi, T. M. Antonsen, Jr., and E. Ott, "The spectrum of fractal dimensions of passively convected scalar gradients in chaotic fluid flows," *Phys. Fluids A* **3**, 1017 (1991).
- ²²J.-P. Eckmann and D. Ruelle, "Ergodic theory of chaos and strange attractors," *Rev. Mod. Phys.* **57**, 617 (1985).
- ²³B. Legras and R. Vautard, "A guide to Liapunov vectors," in *Proceedings of the 1995 ECMWF Seminar on Predictability*, edited by T. Palmer, Reading, U.K., 1996, pp. 143–156.
- ²⁴B. F. Farrell and P. J. Ioannou, "Generalized stability theory. I. Autonomous operators," *J. Atmos. Sci.* **53**, 2025 (1996).
- ²⁵G. Voth, G. Haller, and J. P. Gollub, "Experimental measurements of stretching fields in fluid mixing," *Phys. Rev. Lett.* **88**, 254501 (2002).
- ²⁶B. L. Hua, "The conservation of potential vorticity along Lagrangian trajectories in simulations of eddy-driven flows," *J. Phys. Oceanogr.* **24**, 498 (1994).
- ²⁷X. Z. Tang and A. H. Boozer, "Finite time Lyapunov exponent and advection-diffusion equation," *Physica D* **95**, 283 (1996).
- ²⁸J. L. Thiffeault and A. H. Boozer, "Geometrical constraints on finite-time Lyapunov exponents in two and three dimensions," *Chaos* **11**, 16 (2001).
- ²⁹I. Goldhirsch, P.-L. Sulem, and S. A. Orszag, "Stability and Lyapunov stability of dynamical systems: A differential approach and a numerical method," *Physica D* **27**, 311 (1987).
- ³⁰S. V. Ershov and A. B. Potapov, "On the concept of stationary Lyapunov basis," *Physica D* **118**, 167 (1998).
- ³¹G.-C. Yuan, K. Nam, T. M. Antonsen, Jr., E. Ott, and P. N. Guzdar, "Power spectrum of passive scalars in two dimensional chaotic flows," *Chaos* **10**, 39 (2000).
- ³²A. Okubo, "Horizontal dispersion of floatable particles in the vicinity of velocity singularity such as convergences," *Deep-Sea Res. Oceanogr. Abstr.* **17**, 445 (1970).
- ³³J. Weiss, "The dynamics of enstrophy transfer in two-dimensional hydrodynamics," *Physica D* **48**, 273 (1991).
- ³⁴B. L. Hua and P. Klein, "An exact criterion for the stirring properties of nearly two-dimensional turbulence," *Physica D* **113**, 98 (1998).
- ³⁵B. Eckhardt and D. Yao, "Local Lyapunov exponents in chaotic systems," *Physica D* **65**, 100 (1993).
- ³⁶T. M. Antonsen, Z. Fan, E. Ott, and E. Garcia-Lopez, "The role of chaotic orbits in the determination of power spectra of passive scalars," *Phys. Fluids* **8**, 3094 (1996).
- ³⁷K. Ngan and T. G. Shepherd, "A closer look at chaotic advection in the stratosphere. I. Statistical diagnostics," *J. Atmos. Sci.* **56**, 4153 (1999).
- ³⁸R. T. Pierrehumbert, "Lattice models of advection-diffusion," *Chaos* **10**, 61 (2000).
- ³⁹A. Babiano, G. Boffetta, A. Provenzale, and A. Vulpiani, "Chaotic advection in point vortex models and two-dimensional turbulence," *Phys. Fluids* **6**, 2465 (1994).
- ⁴⁰S. Kida, "Motion of an elliptic vortex in a uniform shear flow," *J. Phys. Soc. Jpn.* **50**, 3517 (1981).
- ⁴¹G. Boffetta, G. Lacorata, G. Redaelli, and A. Vulpiani, "Detecting barriers to transport: A review of different techniques," *Physica D* **159**, 58 (2001).
- ⁴²G. Haller, "Lagrangian coherent structures from approximate velocity data," *Phys. Fluids* **14**, 1851 (2002).
- ⁴³N. Nakamura, "Two-dimensional mixing, edge formation and permeability diagnosed in an area coordinate," *J. Atmos. Sci.* **53**, 1524 (1996).
- ⁴⁴P. H. Haynes and E. Shuckburgh, "Effective diffusivity as a diagnostic of atmospheric transport. 1. stratosphere," *J. Geophys. Res., [Atmos.]* **105**, 22777 (2000).